The Institution of Engineering and Technology WILEY

ORIGINAL RESEARCH PAPER

Mitigation of the mutual dynamic interactions between a direct-current fast charging station and its host distribution grid

Mostafa M. Mahfouz[1,2] | **Reza Iravani[3]**

[1] Electrical Power Department, Faculty of Engineering, Cairo University, Giza, Egypt

[2] Egypt and the Department of Electrical and Computer Engineering, University of Toronto, Toronto, Canada

[3] Department of Electrical and Computer Engineering, University of Toronto, Toronto, Canada

Correspondence
Mostafa M. Mahfouz, Toronto, ON, Canada M5S 3G4.
Email: mostafa.mahfouz@mail.utoronto.ca

Abstract

The fast and intermittent power changes in a direct-current fast charging (DCFC) station impose adverse dynamic impacts on the station's host grid, particularly a weak AC distribution grid. This paper (i) investigates the impacts of the electric vehicle (EV) conventional DCFC station on its host distribution power system, and (ii) shows that the station can be enhanced by a battery energy storage system and an appropriate control strategy to mitigate the mutual dynamic interactions between the station and its host grid. The enhanced DCFC station is based on a variable-voltage, common DC-bus architecture which masks the station's internal dynamics, including rapid and intermittent EV charging processes, from the grid. Thus, it can be interfaced to a host grid, regardless of short-circuit level, X/R ratio, and power capacity. The focus is also on the dynamic immunity of the DCFC facility to potential disturbances in its host weak-grid. The reported studies are based on detailed time-domain simulation of two DCFC stations in the PLECS software platform.

1 | INTRODUCTION

Large-scale adoption of electric vehicles (EVs) has environmental and economic benefits [1]; however, the lack of fast-charging infrastructure, particularly on long routes between cities and in rural areas, hinders large-scale EV utilization.

The weak electrical AC distribution grid, which is characterized by low short circuit level (MVA_{sc}) and low X/R-ratio, hinders the adoption of EV fast-charging stations, rendering simultaneous operation of multiple fast-chargers within a station infeasible. The limited capacity of the legacy distribution system is another bottleneck since each fast-charger requires high power, for example, up to 400 kW, as per CHAdeMO V2.0 protocol [2]. Thus, integrating an EV fast-charging station into a weak AC grid can result in (i) protection system malfunction, (ii) steady-state voltage/frequency regulation problems, and (iii) dynamic voltage regulation issues owing to the intermittent and fast load changes associated with the EV fast charging process.

One approach to address the above issues is to enhance the DCFC station with a battery energy storage system (BESS). Unlike conventional charging stations [4–15], the proposed

BESS-enhanced DCFC station can be interfaced to the legacy AC distribution grid, irrespective of its weaknesses and technical limits [3]. It can mitigate the grid voltage regulation problem by limiting the station's imported power to a pre-specified limit and confine the EV-charging dynamics within the station [3]. A supervisory controller (SC) that controls the BESS charging/discharging, in coordination with the other controllable units within the station, has been reported in [16].

This paper investigates the weak-grid voltage-regulation challenges due to grid-integration of a DCFC station and highlights the technical feasibility of the proposed BESS-enhanced station to mitigate the voltage problems. Based on time-domain simulation studies in PLECS, the dynamic performance of the BESS-enhanced station, under weak-grid conditions and subject to internal and grid-side large-signal disturbances, is investigated. The reported studies include concurrent charging of EVs, DC-bus faults, sudden outages of a supplementary solar-PV unit within the station, grid-side voltage sag, and asymmetrical grid-side faults.

The paper is structured as follows: Section 2 reviews the power and control architectures of the existing DCFC stations.
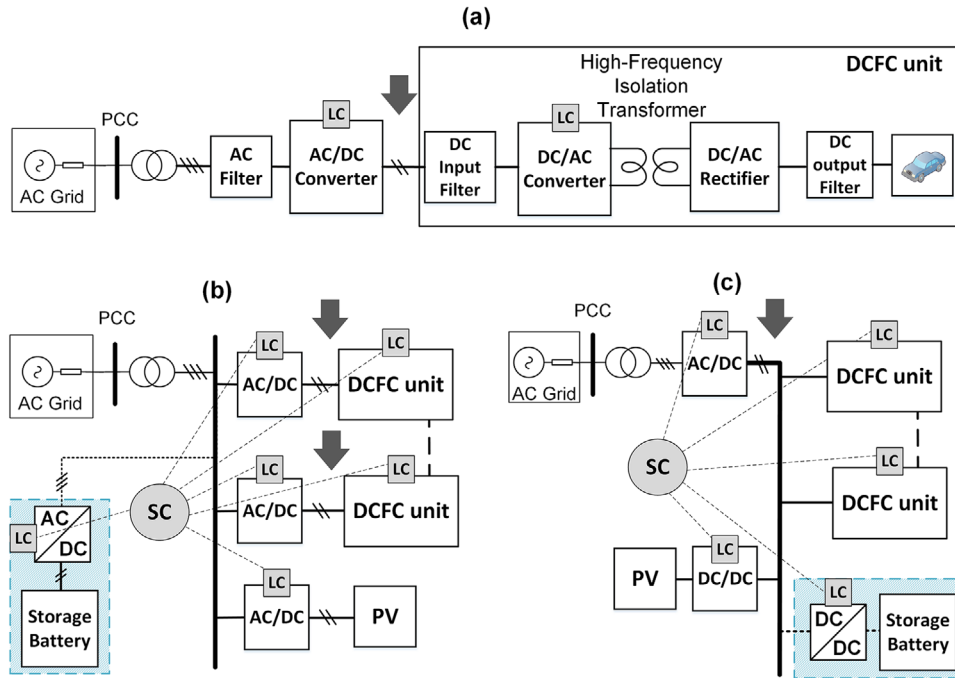
FIGURE 1   Reported DCFC stations' main architectures (a) single-stall unit, (b) common AC-bus architecture, (c) common DC-bus architecture

Section 3 provides the structure and operational concept of the BESS-enhanced DCFC station. Section 4 presents simulation results of conventional and BESS-enhanced stations under weak-grid conditions and large-signal disturbances. Section 5 concludes the paper.

2 | CONVENTIONAL DCFC STATIONS

DCFC units are commercially available in either single-stall units (Figure 1a) or multi-stall DCFC stations. The reported multi-stall DCFC stations can be classified into (i) common AC-bus and (ii) common DC-bus as shown in Figure 1b,c, respectively [4–15]. In the system of Figure 1b, the BESS also can be connected to the PCC instead of the common AC bus. As compared with the configuration of Figure 1b, the common DC-bus architecture of Figure 1c reduces the number of AC/DC conversion stages and thus (i) improve energy conversion efficiency, (ii) reduce complexity, (iii) improve supply power quality due to the absence of reactive power in DC system, and (iv) enhance system reliability by reducing the number of components. We refer to the configurations in Figure 1 as the conventional DCFC stations.

Although stations' architecture may vary, the first objective of their reported control strategies is to regulate the DC voltage of the DCFC units, at the buses identified by arrows in Figure 1. This implies the station's balance of power must be provided by the supply grid. The BESS, in Figure 1b–c, is to mitigate the steady-state impact of the conventional DCFC stations on the grid [4–15]. However, the controls are not intended to address the chargers' dynamic impacts on the grid, particularly when the

host grid is a weak or a moderately weak AC-distribution feeder [17]. The reason is that the response-time associated with the (i) BESS converter's Local Controller (LC), (ii) signal communication to/from the station SC (SC), and (iii) SC processing time is longer than the time frame of the station's dynamic impact on its host grid.

The conventional DCFC stations of Figure 1 suffer from one or more of the following limitations/shortcomings [4–15].

- The station needs to be hosted by a strong AC-grid and thus either the full or partial balance of power for the charging process is imported from the grid.
- The control system neglects the station's impact on the weak-grid dynamics owing to the net time required for the (i) grid-side measurements acquisition, (ii) signal communication to SC, (iii) processing by SC, and (iv) communication of the SC signal to the LC.
- The station's control system does not provide robustness to the station's operating point and parameters uncertainties, for example, the BESS and/or EVs charging/discharging voltages/currents and the host feeder parameters.
- The number of DCFC units within the station is pre-determined and cannot be changed without modifying the station's control system. This is a major impediment to the station's expansion and maintenance process.

The convention DCFC station of Figure 1b, excluding the BESS in the shaded box, is used in this work as the benchmark to investigate and quantify the impacts of the conventional DCFC station on the grid. It employs (i) four DCFC units where each unit provides up to 125 kW within the voltage range
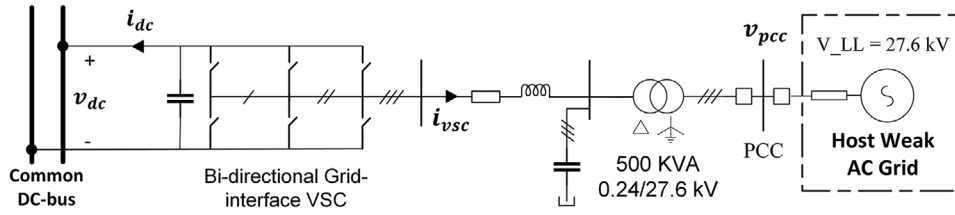
FIGURE 2 Schematic diagram of grid-interface VSC and the supply grid for the conventional DCFC station
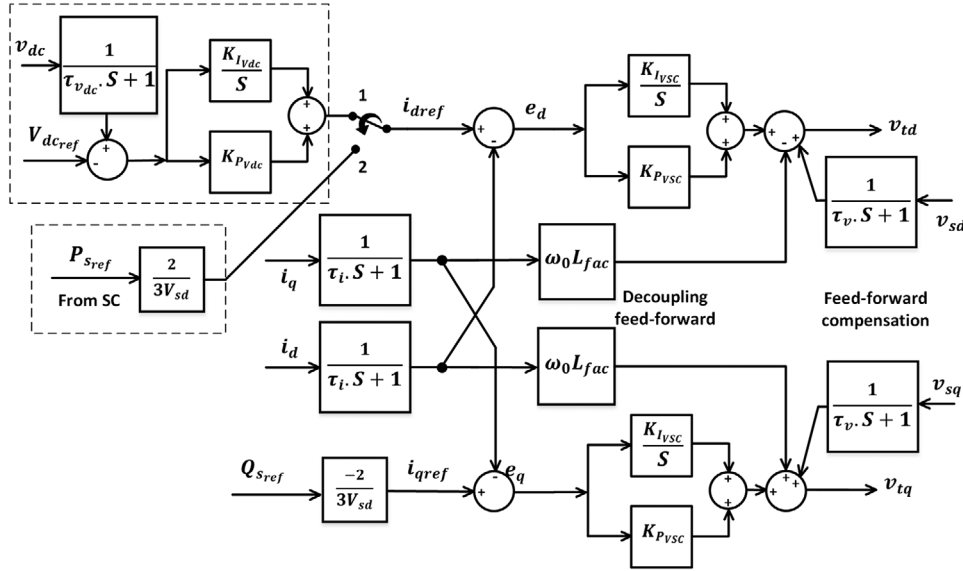

FIGURE 3 Structure of the LC of the VSC in conventional and BESS-enhanced stations

of 200–500 V to its EV load, (ii) one 50 kW PV unit, and (iii) one 500 kW, grid-interface, three-phase AC-DC voltage-sourced converter (VSC).

Figure 2 shows a schematic diagram of the grid-interface AC-DC VSC of Figure 1b and its grid equivalent subsystem [3, 18]. The three-phase, two-level VSC [18] operates based on a 7.2 kHz, SPWM switching strategy and is synchronized to the grid voltage at the low-voltage side of the coupling transformer by a phase-locked loop [3, 18]. The host grid with respect to the PCC is represented by the equivalent circuit of a 27.6 kV radial feeder and its upstream supply system [17]. The VSC adopts the inner-loop current controller and the outer DC-bus voltage controller as shown in Figure 3, with the switch in position '1'. The VSC operates at unity power factor (PF), that is, $Q_{S_{ref}} = 0$, and its DC-side voltage is regulated at 600 V, that is, $V_{dc_{ref}} = 600$ V.

Figure 4 shows that each DCFC unit of the conventional station comprises: (i) an input DC filter, (ii) a unidirectional galvanically isolated, 50 kHz phase-shifted full-bridge (PSFB) converter [19] and an output DC filter, (iii) the EV battery [20], and (iv) a current controller [21]. Subsequent to connection to the EV system and prior to the charging process, the charger receives data from the battery management system (BMS) of the EV, for example, the charge level, battery voltage, and desired charging current [22]. The data is exchanged throughout the charging process and the charging current command from the EV BMS "i_{ref_i}" dynamically changes. In the conventional station of Figure 1b:

- Each DCFC unit fully satisfies the charging requirements (current and voltage) of its corresponding EV.
- The solar-PV unit operates in the maximum power point tracking (MPPT) mode and behaves as a time-varying power source. The output power of the solar-PV unit can change abruptly owing to moving clouds and fast changes in irradiance.
- The VSC fully relies on the host AC-grid to supply the station's balance of power to maintain the DC-bus voltage at the desired value, that is, 600 V.

3 | BESS-ENHANCED DCFC STATION

Figure 5 depicts the BESS-enhanced DCFC station. In addition to the subsystems described for the conventional DCFC station of Figure 2b, the DCFC station of Figure 5 also employs one 450–600 V, 1 MWh BESS which is directly connected to the common DC bus, and the DC bus voltage fluctuates within
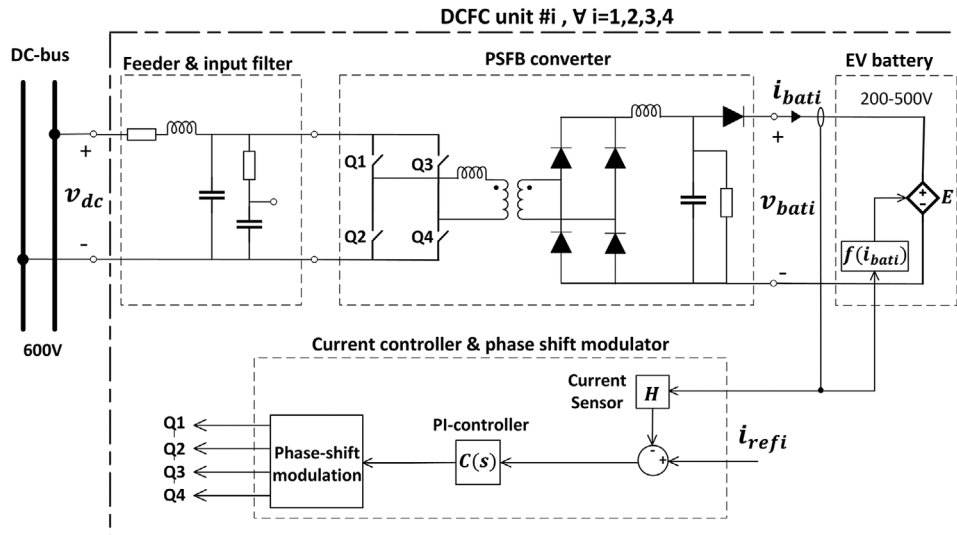
FIGURE 4   Circuit diagram of one DCFC unit connected to the DC bus
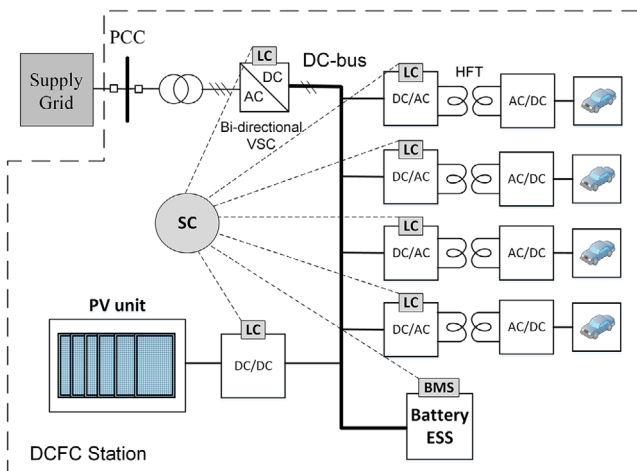

FIGURE 5   Power and control structure of the BESS-enhanced DCFC station

450–600 V, based on the SOC of the BESS [20]. It should be noted that the DC-bus voltage of the conventional DCFC station of Figure 1b is regulated at 600 V.

A two-layer control system, that is, LCs and an SC, enables the operation of the DCFC station of Figure 5. The station uses the same DCFC units as those of the conventional station as shown in Figure 4. The outer LC loop of the VSC of the station is based on open-loop power control as shown in Figure 3, with switch in position '2'. The SC limits the active power imported to the station depending on the technical limits of the supply grid at the PCC and sets reactive power command to zero for unity power factor operation.

For a given EV charging demand and PV output power, the SC of Figure 5 determines the operational modes of each DCFC unit, the PV unit, and the grid-interface VSC, based on the state of charge (SOC) and charging/discharging rate of the BESS [16]. For example:(i) each DCFC unit can either fully provide or curtail the charging power of the corresponding EV, (ii) the PV

system can operate in either MPPT mode or curtailment mode, and (iii) the grid-interface VSC determines power exchange with the grid by adjusting the LC active and reactive power setpoints of the VSC. The SC also limits the station's imported power to a predefined value, based on the grid strength. The development and detailed operation of the SC is presented in [16].

4 | STUDY RESULTS AND DISCUSSION

The PLECS software platform is used for time-domain simulation, including switched-model of the converters [24], to evaluate internal (inside the station) and external (grid-side) nonlinear dynamic behaviour of the conventional DCFC station and the BESS-enhanced DCFC station of Figure 1b,5, respectively. The reported case studies include:

- simultaneous charging of four EVs each at the rated power of the corresponding charger, under different weak-grid conditions;
- a sudden loss of the solar-PV unit power;
- a temporary DC-bus fault;
- a grid-side voltage sag;
- a temporary asymmetrical grid-side fault.

4.1 | Simultaneous charging of multiple EVs

This case study shows dynamic responses of the DCFC stations of Figure 1b,5 to simultaneous charging of EVs under different MVA_{sc} and X/R ratios of the grid. Initially, (i) the charging units provide no power to the EVs, (ii) the solar PV-unit injects no power to the station's DC bus, and (iii) the grid-interface VSC imports zero power and 120 kW in the DCFC stations of Figure 1b,5, respectively. The four EVs request charging at 250 A and 391 V each, at $t = 0.1, 0.5, 0.9,$ and 1.3 s, respectively.
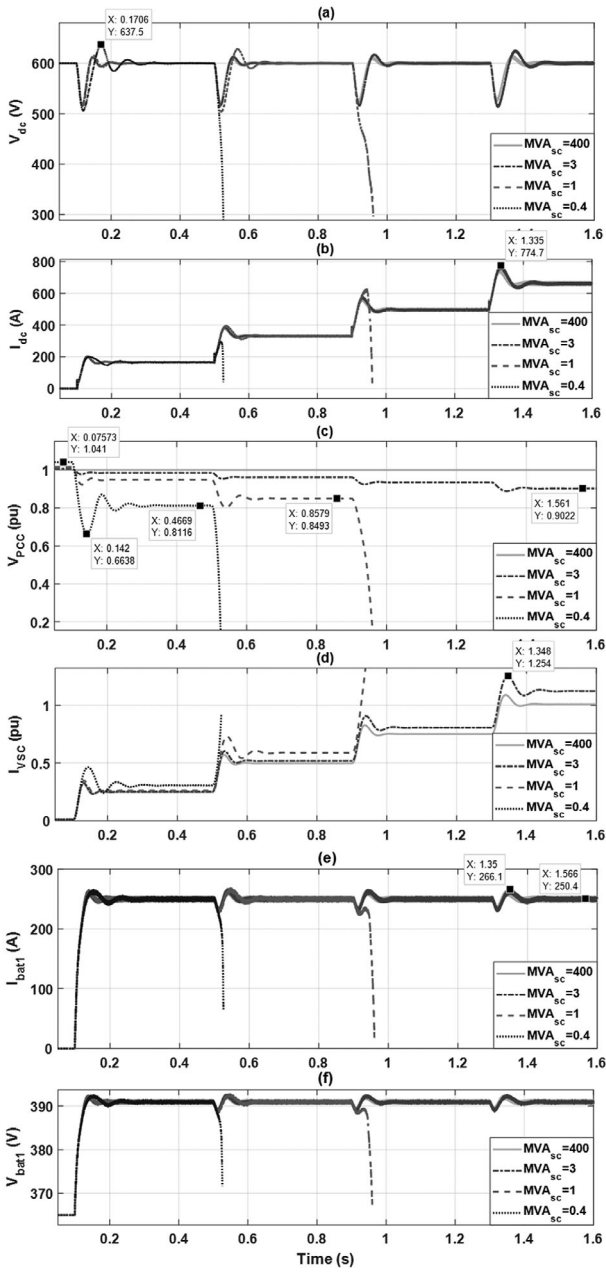
FIGURE 6 Simultaneous charging of four EVs in the conventional station under different grid MVA_{sc} levels and fixed $X/R = 1.4$ (a) DC bus voltage, (b) station-imported DC current, (c) PCC voltage phasor magnitude in per unit, (d) VSC AC-side current phasor magnitude in per unit, (e) charging current of the first EV, (f) charging voltage of the first EV

4.1.1 | Conventional station of Figure 1b ($X/R = 1.4$)

Figure 6 shows the study results under the fixed $X/R = 1.4$ at MVA_{sc} of 400, 3, 1, and 0.4 MVA. Figure 6a shows that for $MVA_{sc} = 400$ and even $MVA_{sc} = 3$, the grid-interface VSC regulates the DC-bus voltage at 600 V by relying on the grid to fully provide the balance of power as given in Figure 6b. Figure 6c,d illustrates that simultaneous charging of EVs requires higher current from the supply grid and results in a

larger PCC voltage drop. Figure 6e,f shows the output current and voltage of the first DCFC unit. For $MVA_{sc} = 400$ and $MVA_{sc} = 3$, Figure 6e,f depicts that the first DCFC unit is able to regulate its EV charging current and voltage at the desired values of 250 A and 391 V, despite charging initiation of three additional EVs at times 0.5, 0.9, and 1.3 s.

Figure 6c shows that for $MVA_{sc} = 1$, upon charging of the second EV, the steady-state grid voltage at PCC drops to 0.85 pu and violates the steady-state voltage limit [23]. Figure 6 shows, when the third EV starts charging, (i) the DC-bus voltage controller no longer can regulate the DC-bus voltage (Figure 6a), (ii) the LCs of the DCFC units fail to maintain the EVs charging requirement (Figure 6e,f), and (iii) the protection system would trip the station. This implies under the given weak grid condition, the only operation of one charging unit, at a time, in the conventional DCFC station is permitted.

As depicted in Figure 6c, for $MVA_{sc} = 0.4$, the PCC voltage of the conventional station (i) violates the steady-state voltage limit upon charging of even one EV and (ii) collapses when the second EV starts charging. This indicates under the given weak-grid condition of $MVA_{sc} = 0.4$, the conventional station cannot meet the EVs charging requirements. Figure 6 concludes that for a fixed feeder's X/R ratio, the lower the grid MVA_{sc} level (the weaker the grid), the more severe the voltage regulation problem is and the more challenging it is to interface the station of Figure 1b to the grid.
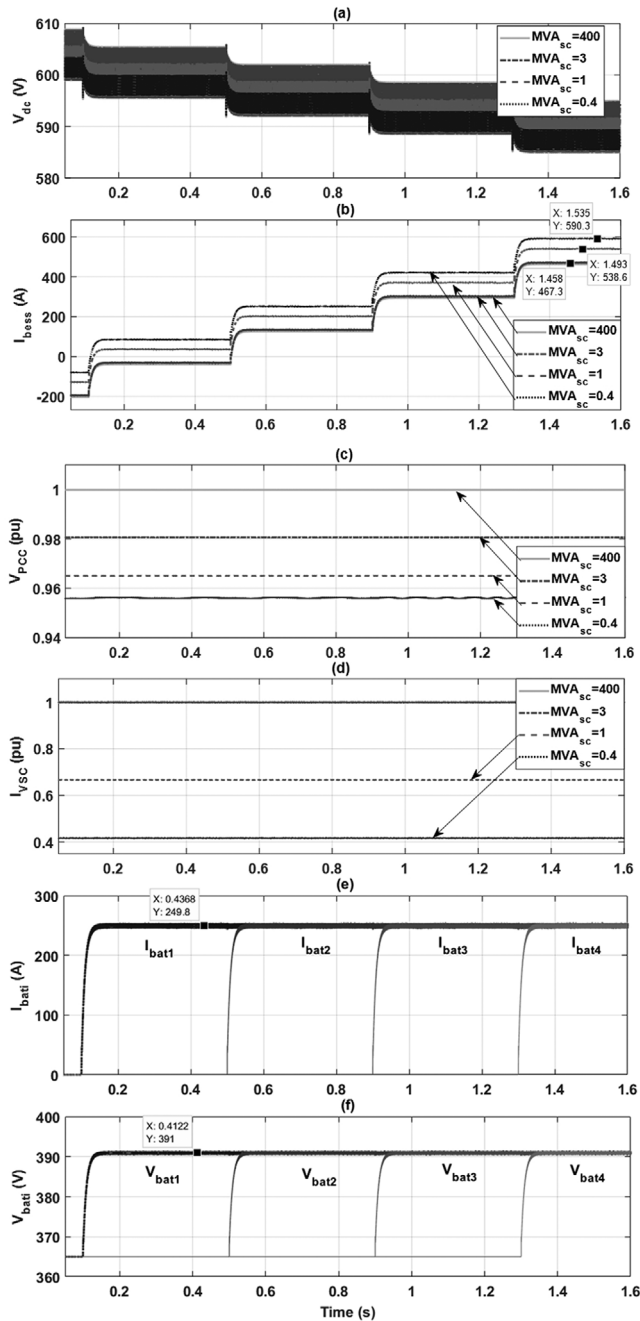
4.1.2 | BESS-enhanced station of Figure 5 ($X/R = 1.4$)

Figure 7 shows the study results of the BESS-enhanced station under the grid $X/R = 1.4$ at MVA_{sc} of 400, 3, 1, and 0.4 MVA. Based on the grid requirement, the station imported power is limited to 120, 80, and 50 kW corresponding to $MVA_{sc} = 3$ (and higher), 1, and 0.4, respectively. Figure 7a shows that when more EVs simultaneously charge, the DC bus voltage reduces to a lower value due to the increase in voltage drop across the BESS internal resistance. Figure 7b shows the station relies on the BESS, instead of the grid, to maintain the balance of power. Figure 7c,d shows that the grid-side voltage and the VSC AC-side currents are not affected by simultaneous charging of EVs. Figure 7e,f shows the EVs charging currents and voltages are tightly regulated at their setpoints and the DCFC units' operations are not coupled to each other's. This highlights the salient feature that enables adding more DCFC units to the station, without the need to redesign/readjust the station's existing LCs. Comparison of Figures 6 and 7 conclude the BESS-enhanced station and its control system enable its integration in a weak grid regardless of the MVA_{sc} level.

4.1.3 | Conventional station of Figure 1b ($MVA_{sc} = 1.2$)
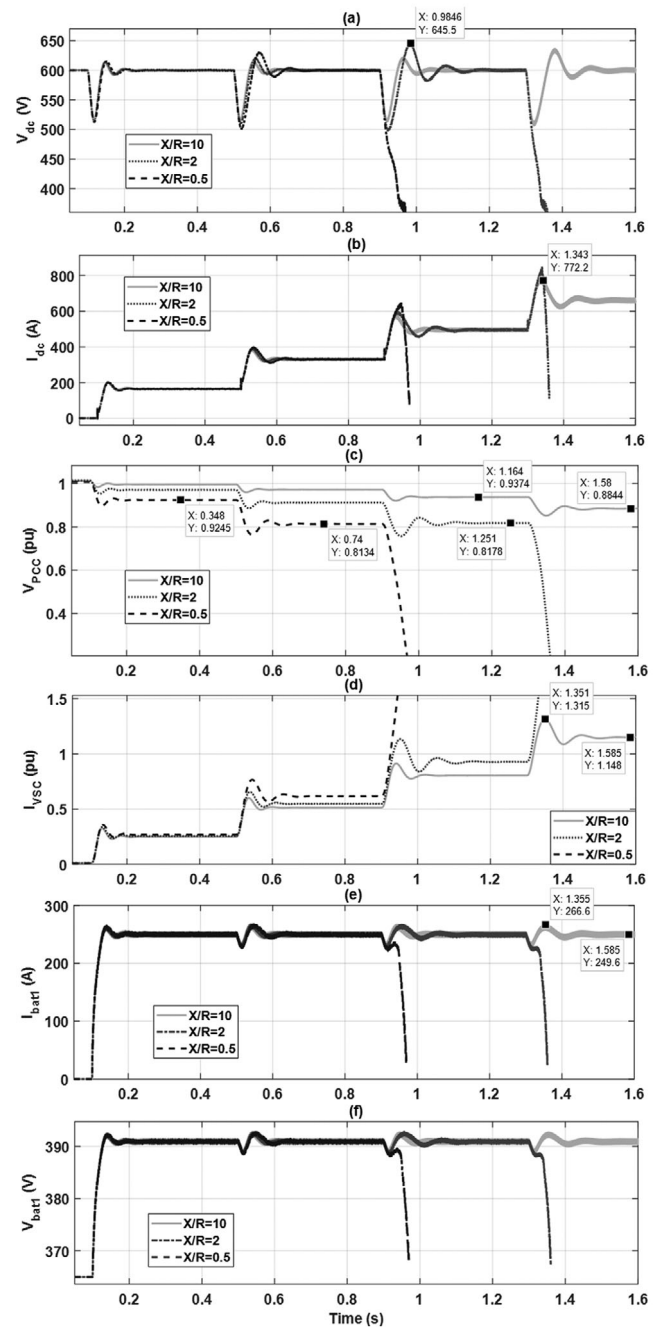
Figure 8 shows the study results of the conventional station under $MVA_{sc} = 1.2$ at X/R ratios of 10, 2, and 0.5. Figure 8a

FIGURE 7 Simultaneous charging of four EVs in BESS-enhanced station under different grid MVA_{sc} levels and fixed $X/R = 1.4$ (a) DC bus voltage, (b) BESS discharge current, (c) PCC voltage phasor magnitude in per unit, (d) VSC AC-side current phasor magnitude in per unit, (e) EVs' charging currents, (f) EVs' charging voltages

FIGURE 8 Simultaneous charging of four EVs in 'conventional' under fixed $MVA_{sc} = 1.2$ and different X/R ratios (a) DC bus voltage, (b) station-imported DC current, (c) PCC voltage phasor magnitude in per unit, (d) VSC AC-side current phasor magnitude in per unit, (e) charging current of first EV, (f) charging voltage of the first EV

shows at $X/R = 10$, the grid-interface VSC regulates the station's DC-bus voltage at 600 V by relying on the grid to provide the full balance of power as shown in Figure 8b. Figure 8c shows for $X/R = 10$, during the charging of the fourth EV, the steady-state grid voltage at PCC drops to 0.88 pu and violates the voltage limit [23]. Moreover, Figure 8d shows that the VSC current increases above 1 pu to supply the EVs charging power despite the reduction in the grid voltage. Thus, the

conventional station behaves as a constant power load with respect to the grid. Figure 8e,f shows the four EVs can be simultaneously charged at the requested currents and voltages.

At $X/R = 0.5$, upon charging of the second EV, Figure 8c shows that the steady-state grid voltage at PCC drops to 0.813 pu which violates the minimum permissible steady-state voltage [23]. When the third EV starts charging (i) Figure 8a shows the DC-bus voltage controller can no longer regulate the

DC-bus voltage, (ii) Figure 8e,f show the LCs of the DCFC units fail to maintain the EVs charging currents and voltages at their setpoints, and (iii) the under-voltage protection would trip the station. This implies that under the given weak grid condition, the operation of only one DCFC unit in the conventional DCFC station is permitted. Figure 8 concludes that, for a fixed level of grid MVA_{sc}, the lower the supply feeders X/R ratio, the more severe the voltage regulation problem is and thus, it is more challenging to interface the conventional DCFC station to the grid.

4.1.4 | BESS-enhanced station of Figure 5 ($MVA_{sc} = 1.2$)

Figure 9 shows the study results under $MVA_{sc} = 1.2$ at X/R ratios of 10, 2, and 0.5. Based on the grid requirement, the imported power from the grid is limited to 80 kW. Figure 9a shows the DC bus voltage drop when different number of charging units are operational and Figure 9b shows that the station relies on the BESS to maintain the balance of power. Figure 9c,d shows the grid-side voltage and the VSC AC-side currents are not affected by the simultaneous charging of EVs. Figure 9e,f show the EVs charging currents and voltages are regulated at their setpoints. As compared with Figure 8,9 concludes that the BESS-enhanced station and its control system enable its integration in a weak grid regardless of the X/R ratio.

4.2 | Disturbance in solar-PV output power

This case study assumes $MVA_{sc} = 3$ at the PCC of the AC-grid and $X/R = 1.4$. Initially (i) the four DCFC units charge the corresponding EVs at (130 A, 433.5 V), (150 A, 406 V), (170 A, 377.5 V), and (190 A, 350 V) respectively, (ii) the PV unit provides 50 kW to the DC-bus, (iii) the grid-interface VSC of the conventional station of Figure 1b imports 200 kW and the VSC of the BESS-enhanced station of Figure 5 imports 120 kW from the grid. Figure 10 shows dynamic responses of the two stations to a tripping of the solar-PV unit and the loss of 50 kW output power of the PV unit at $t = 0.05$ s.

For the conventional station, Figure 10a shows the DC-bus voltage decreases to 540 V subsequent to the disturbance, before the DC-bus voltage controller brings the voltage to 600 V. Figure 10b,d illustrates that the conventional station grid-side current (and power) increases to compensate for the loss of solar PV power and thus the grid-PCC voltage drops as shown in Figure 10c. Figure 10e shows EVs charging currents overshoot by approximately 7% as a result of the PV power disturbance and then are regulated at their setpoint values.

For the BESS-enhanced station of Figure 5, Figure 10b shows the BESS discharge current increases to compensate for the loss of the PV unit power and thus the DC bus voltage of Figure 10a slightly decreases due to the increase in voltage drop across the BESS internal resistance. Figure 10c,d shows that the grid-voltage and the VSC AC-side currents are not affected by the sudden drop in the PV unit power. This demonstrates capability
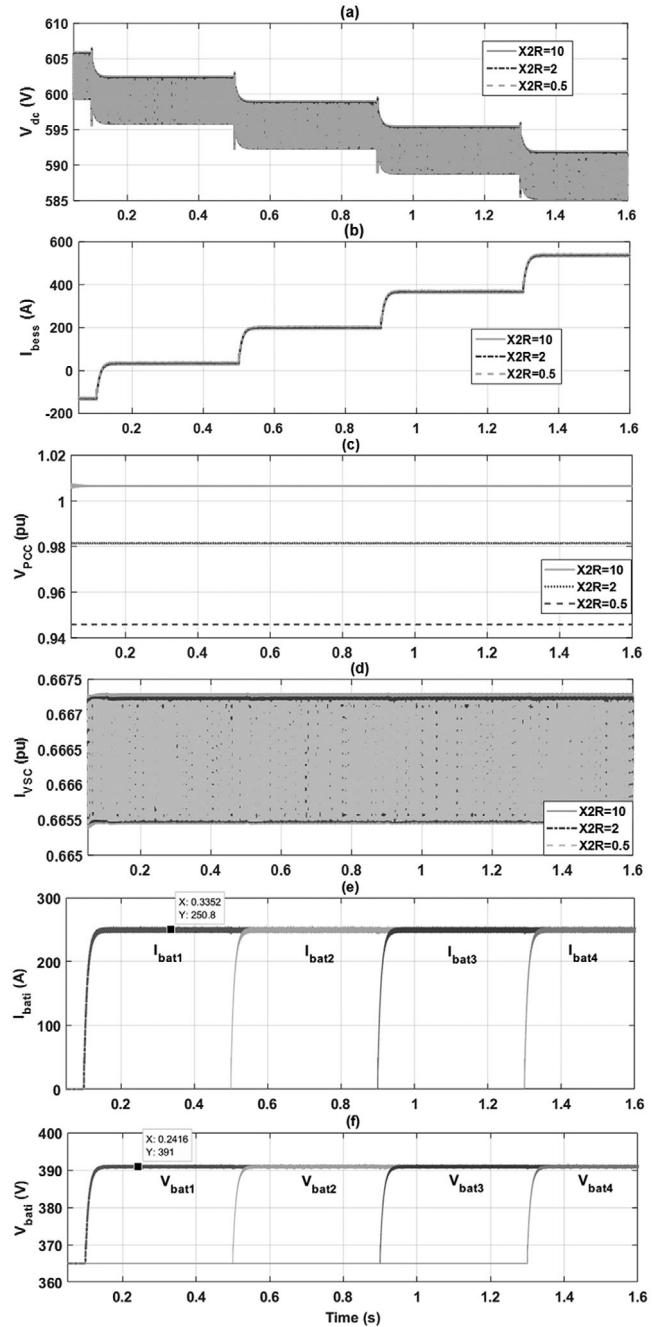
FIGURE 9 Simultaneous charging of four EVs in "BESS-enhanced" under fixed $MVA_{sc} = 1.2$ and different X/R ratios (a) DC bus voltage, (b) BESS discharge current, (c) PCC voltage phasor magnitude in per unit, (d) VSC AC-side current phasor magnitude in per unit, (e) EVs' charging currents, (f) EVs' charging voltages

of the BESS-enhanced station to mask the PV power disturbances from the host grid. Figure 10e,f shows, unlike the conventional station, the PV power disturbance has no significant impact on the EVs' charging currents and voltages.

Figure 10 concludes the BESS-enhanced station of Figure 5, unlike that of Figure 1b, prevents the steady state and dynamic impacts of the solar PV-power disturbances on the host weak grid and the EVs' charging currents/voltages.
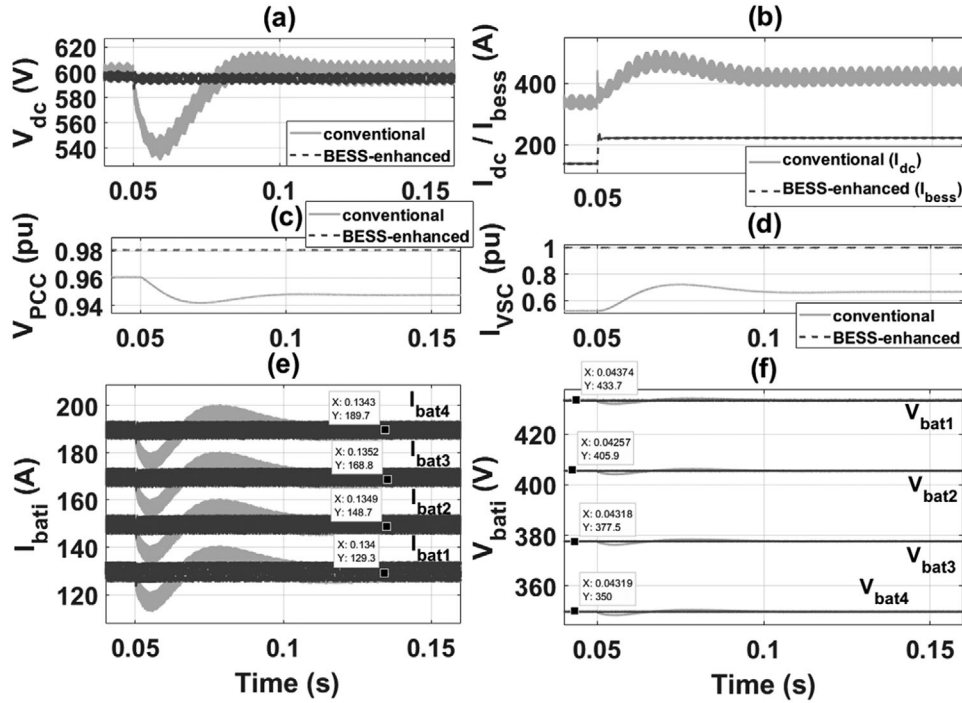
FIGURE 10 System response to 50 kW decrease in solar-PV unit power at $t = 0.05$ s
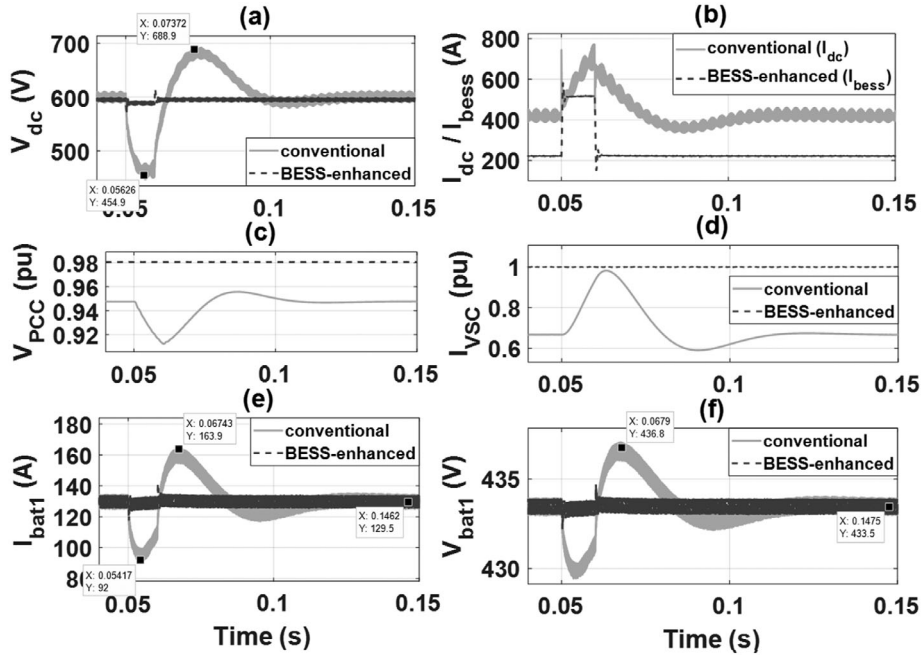

FIGURE 11 Temporary 10 ms DC-bus fault at $t = 0.05$ s

4.3 | Temporary DC-bus fault

This case study assumes $MVA_{sc} = 3$ at the PCC of the AC-grid and $X/R = 1.4$. Initially (i) the four DCFC units charge their EVs at (130 A, 433.5 V), (150 A, 406 V), (170 A, 377.5 V), and (190 A, 350 V) respectively, (ii) the PV unit supplies

no power, (iii) the grid-interface VSC imports about 250 and 120 kW from the host grids of the conventional and the BESS-enhanced stations, respectively. This case investigates dynamic behaviours of the station of Figure 1b and the station of Figure 5 due to a 10 ms DC-bus fault with the fault resistance of 2 Ω, at $t = 0.05$ s.
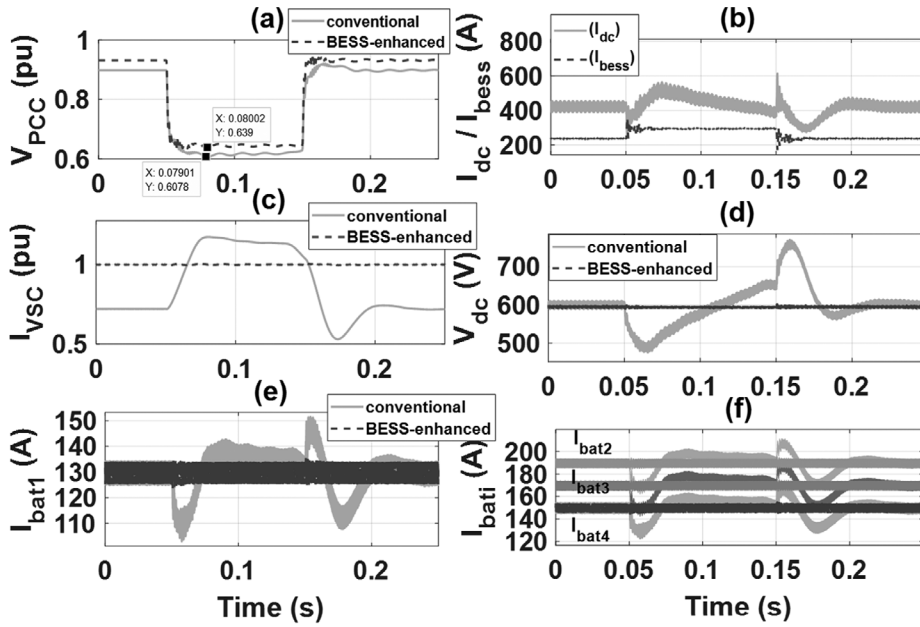
FIGURE 12 A 100 ms grid-side voltage sag at $t = 0.05$ s

The fault reduces the DC-bus voltage as shown in Figure 11a. Figure 11b shows the grid-VSC of Figure 1b draws a large current from the grid 'I_{dc}' to compensate for the power dissipated in the fault resistance and to retain the DC-bus voltage at the desired value. However, in the station of Figure 5, the BESS discharge current increases and results in a 2% voltage drop across the BESS's internal resistance. Figure 11c,d depicts the decrease in the PCC voltage due to the increase in the imported VSC current of the station of Figure 1b, however, the VSC current in the BESS-enhanced station is tightly regulated and thus the grid-voltage remains unaffected by the fault. Figure 11e shows, in the station of Figure 1b, the EV charging current decreases by 30% and increases by 26% at the fault inception and clearance instants, respectively. This can activate the DCFC unit's protection and disrupts the EV charging. However, in the BESS-enhanced station of Figure 5, the EV charging dynamics are not noticeably affected by the DC-bus voltage drop as a result of the fault. Figure 11 concludes that the BESS-enhanced station of Figure 5, unlike the conventional station of Figure 1b, conceals its internal faults and mitigates their impacts on the (i) host grid dynamics and (ii) EVs' charging currents/voltages.

4.4 | Grid-side voltage sag

This case study assumes $MVA_{sc} = 3$ at the PCC of the AC-grid and $X/R = 1.4$. Initially (i) the four DCFC units charge their EVs at (130 A, 433.5 V), (150 A, 406 V), (170 A, 377.5 V), and (190 A, 350 V) respectively, (ii) the PV unit provides zero power to the DC-bus, (iii) the grid-interface VSC imports about 250 and 120 kW from the host grid of the conventional and the BESS-enhanced stations, respectively. This case study evaluates performance of the conventional and the BESS-enhanced

DCFC stations to a 100 ms grid-side voltage sag following a three-phase-to-ground fault in the upstream supply feeder, at $t = 0.05$ s.

Figure 12a shows that, during the voltage sag interval, the voltage at PCC dips to 0.6 and 0.63 pu for the conventional and the BESS-enhanced DCFC stations, respectively. Figure 12b shows the station imported DC current and the BESS discharge current for the conventional station and BESS-enhanced station, respectively. Despite the grid-voltage disturbance, Figure 12c shows that the VSC of the BESS-enhanced station maintains the VSC AC-side current at 1pu, even during the voltage sag interval. Figure 12d shows that a grid-side voltage sag has less impact on the station's DC-bus voltage in the BESS-enhanced station as compared with the conventional station. Similarly, Figure 12e,f show that EVs' charging currents in the BESS-enhanced station remain unchanged during the voltage sag. This implies that EVs' charging dynamics are less sensitive to the grid-side voltage disturbances in the BESS-enhanced DCFC station than the conventional station.

4.5 | Temporary asymmetrical grid-side fault

The initial operating condition in this case study is identical to the previous grid-side voltage sag scenario. However, this case study investigates dynamic behaviour of the conventional and the BESS-enhanced DCFC stations subject to a 50 ms, single-line-to-ground fault at PCC, at $t = 0.05$ s.

Figure 13a,c show the magnitudes of the PCC voltage and VSC AC-side current phasors. Figure 13b shows the station imported DC current and the BESS discharge current for the conventional station and BESS-enhanced station, respectively. The reason for the damped-beating in Figure 13b, subsequent
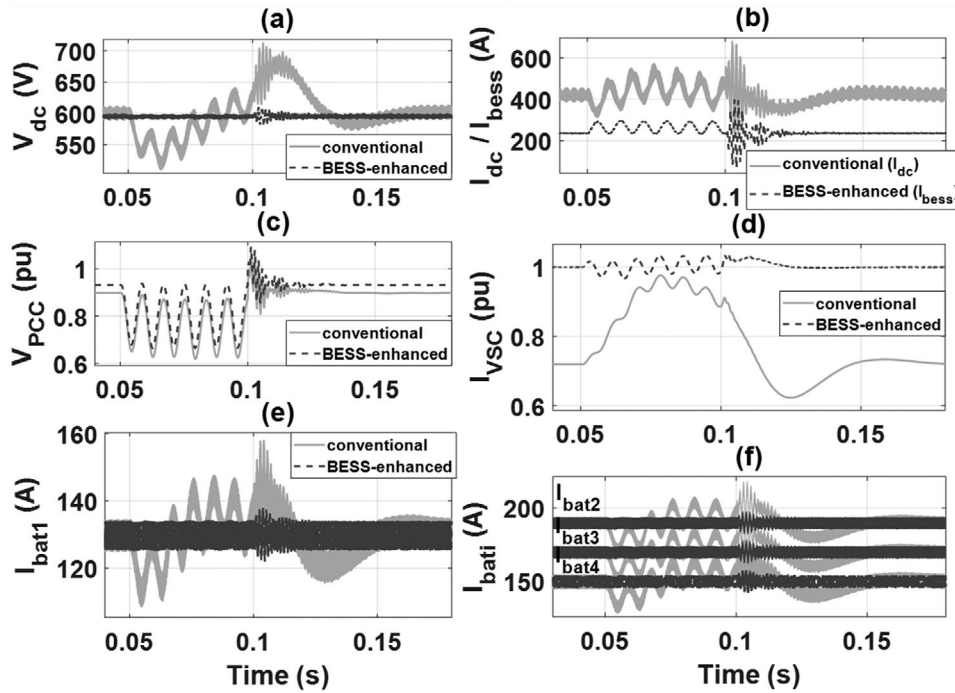
FIGURE 13 Temporary 50 ms single-line-to-ground fault at PCC at $t = 0.05$ s

to fault clearance (at $t = 0.1$ s), is the presence of two oscillatory modes with close natural frequencies [3]. The reason for the 120 Hz ripple component is the presence of the negative sequence component in both current and voltage during the asymmetrical fault. Figure 13c shows that the VSC of the BESS-enhanced station, unlike the conventional station, regulates the positive sequence component of VSC AC-side current at 1 pu, even during the fault interval.

Due to the unbalanced operation during the fault, Figure 13d depicts a significant 120 Hz ripple component in the DC-bus voltage of the conventional station as compared to that of the BESS-enhanced station. Similarly, Figure 13e,f show that EVs charging currents in the BESS-enhanced station are not noticeably affected by the asymmetrical fault (at the fault instant, during the fault, and subsequent to the fault clearance) as compared to that of the conventional station.

This case study demonstrates the capability of the BESS-enhanced station to connect to an unbalanced three-phase (or even a single phase) supply grid without detrimental impact on EVs' charging processes and highlights the BESS-enhanced station can withstand temporary unbalanced conditions, e.g., asymmetrical grid-side faults, and maintain the EVs' charging currents and voltages.

5 | CONCLUSION

This paper evaluates a BESS-enhanced DCFC station for EVs and highlights the main features of the BESS-enhanced station as compared to a conventional station. The paper shows that a conventional station can operate without a detrimental effect when hosted by a strong grid and thus the balance (or partial balance) of power for the charging process can be extracted from the grid. In contrast, the architecture and controls of the BESS-enhanced station (i) enable connection even to a weak (single or three-phase) feeder and (ii) limit the imported power from the feeder to a pre-specified allowable value. Thus, (i) prevents steady-state impacts on the host feeder, and (ii) the combination of local and supervisory controls contains the station dynamics within the station and prevents the dynamic impacts of the DCFC units and other internal sources, such as solar-PV generation, on the host grid.

The paper also shows that, unlike a conventional station, the control system of the BESS-enhanced station maintains the EVs charging currents and voltages transients within permissible limits, when subjected to the grid-side voltage disturbances and unbalanced operation. Furthermore, the BESS-enhanced station enables a modular structure, that is, the number of charging units can be changed based on the market demand, without the need to change the power or control circuits of either the DCFC converters or the grid-interface VSC. This feature cannot be incorporated in the conventional station, unless the power/control of the grid-interface VSC system is modified accordingly.

REFERENCES

1. Su, W., et al.: A survey on the electrification of transportation in a smart grid environment. in IEEE Trans. Ind. Inf. 8(1), 1–10 (2012)
2. Chademo Association: CHAdeMO releases the latest version of the protocol enabling up to 400 kW. [online]. Available: https://www.chademo.com/chademo-releases-the-latest-version-of-the-protocol-enabling-up-to-400kw (2018)

3. Mahfouz, M.M., Iravani, M.R.: Grid-integration of battery-enabled DC fast charging station for electric vehicles. IEEE Trans. Energy Convers. 35(1), 375–385 (2020)

4. Joos, G., de Freige, M., Dubois, M.: Design and simulation of a fast charging station for PHEV/EV batteries. In: 2010 IEEE Electrical Power & Energy Conference, Halifax, NS, Canada, 25–27 August 2010

5. Bai, S., Lukic, S.M.: Unified active filter and energy storage system for an MW electric vehicle charging station. IEEE Trans. Power Electron. 28(12), 5793–5803 (2013)

6. Aggeler, D., et al.: Ultra-fast DC-charge infrastructures for EV-mobility and future smart grids. In: 2010 IEEE PES Innovative Smart Grid Technologies Conference Europe (ISGT Europe), Gothenberg, Gothenburg, Sweden, 11–13 October (2010), pp. 1–8

7. Veneri, O., et al.: Charging infrastructures for EV: Overview of technologies and issues. In: 2012 Electrical Systems for Aircraft, Railway and Ship Propulsion, Bologna, Italy, 16–18 October (2012), pp. 1–6

8. Sbordone, D., et al.: EV fast charging stations and energy storage technologies: A real implementation in the smart micro grid paradigm. Electr. Power Syst. Res. 120, 96–108 (2015)

9. García-Triviño, P., Torreglosa, J.P., Ramírez, L.M.: Control and operation of power sources in a medium-voltage direct-current microgrid for an electric vehicle fast charging station with a photovoltaic and a battery energy storage system. Energy 115(part1), 38–48 (2016)

10. Wajahat, K., Furkan, A., Alam, M.S.: Fast EV charging station integration with grid ensuring optimal and quality power exchange. Eng. Sci. Technol. Int. J. 22(1), 143–152 (2019)

11. González, L.G., Siavichay, E., Espinoza, J.L.: Impact of EV fast charging stations on the power distribution network of a Latin American intermediate city. Renewable Sustainable Energy Rev. 107, 309–318 (2019)

12. Ashique, R.H., et al.: Integrated photovoltaic-grid dc fast charging system for electric vehicle: A review of the architecture and control. Renewable Sustainable Energy Rev. 69, 1243–1257 (2017)

13. Savio, D.A., et al.: Photovoltaic integrated hybrid microgrid structured electric vehicle charging station and its energy management approach. Energies 12(1), 168 (2019)

14. Srdic, S., Lukic, S.: Toward extreme fast charging: Challenges and opportunities in directly connecting to medium-voltage line. IEEE Electrif. Mag. 7(1), 22–31 (2019)

15. Iunnissi, S.A.: Architecture and control of an electric vehicle charging station using a bipolar DC bus. PhD thesis, Ryerson University (2016)

16. Mahfouz, M.M., Iravani, R.: A supervisory control for resilient operation of the battery-enabled DC fast charging station and the grid. IEEE Trans. Power Delivery 36, 2532–2541, https://doi.org/10.1109/TPWRD.2020.3031859

17. Hayhoe, A.: Impact of irradiance change on MPPT and flicker phenomenon of solar-PV units. M.S. thesis, University of Toronto (2016)

18. Mahfouz, M.M., El-Deib, A.A., El-Marsafawy, M.: Modeling and stability assessment of AC microgrids using time-domain simulations. In: 2016 IEEE International Conference on Power System Technology (POWERCON), Wollongong, Wollongong, NSW, Australia, 28 September–1 October 2016

19. Sabate, J.A., et al.: Design considerations for high-voltage high-power full-bridge zero-voltage-switched PWM converter. Fifth Annual Proceedings on Applied Power Electronics Conference and Exposition, Los Angeles, CA, USA, 11–16 March 1990

20. Tremblay, O., Dessaint, L.-A., Dekkiche, A.-I.: A generic battery model for the dynamic simulation of hybrid electric vehicles. Vehicle Power and Propulsion Conference, Arlington, TX, USA, 9–12 September 2007

21. Erickson, R.W., Maksimovic, D.: Fundamentals of Power Electronics. Springer; New York, NY, USA (2001)

22. Quebec, H.: Electric Vehicle Charging Stations Technical Installation Guide. [Online]. Aug 2015, Available: http://www.hydroquebec.com/data/electrification/transport/pdf/technical-guide.pdf

23. North American Electric Reliability Corporation: Performance of Distributed Energy Resources During and After System Disturbance (Voltage and Frequency Ride-Through Requirements) Dec 2013

24. Mahfouz, M.M.: Control and operation of the battery-enabled direct-current fast charging station for electric vehicles. Ph.D. thesis, University of Toronto (2020)